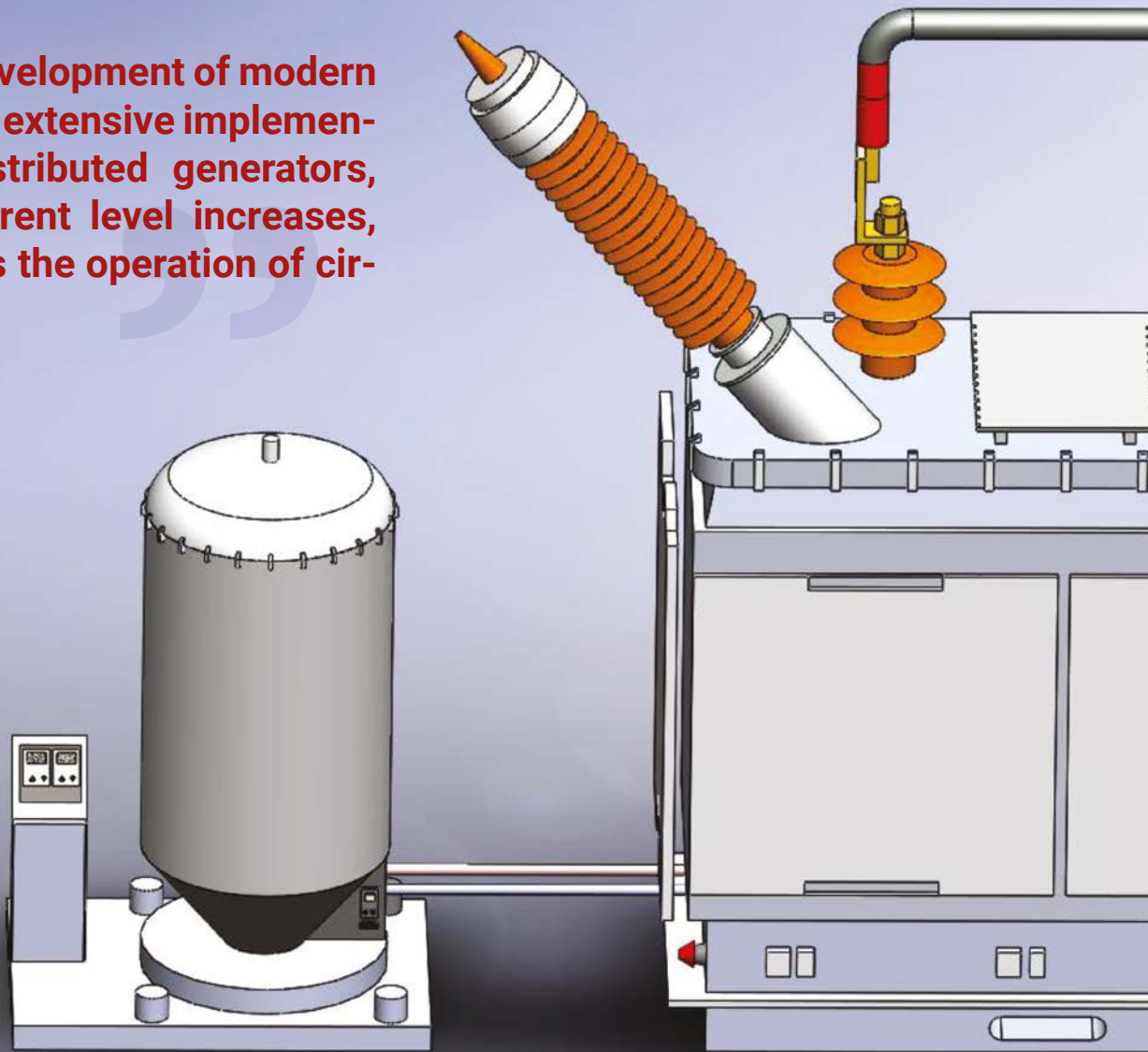
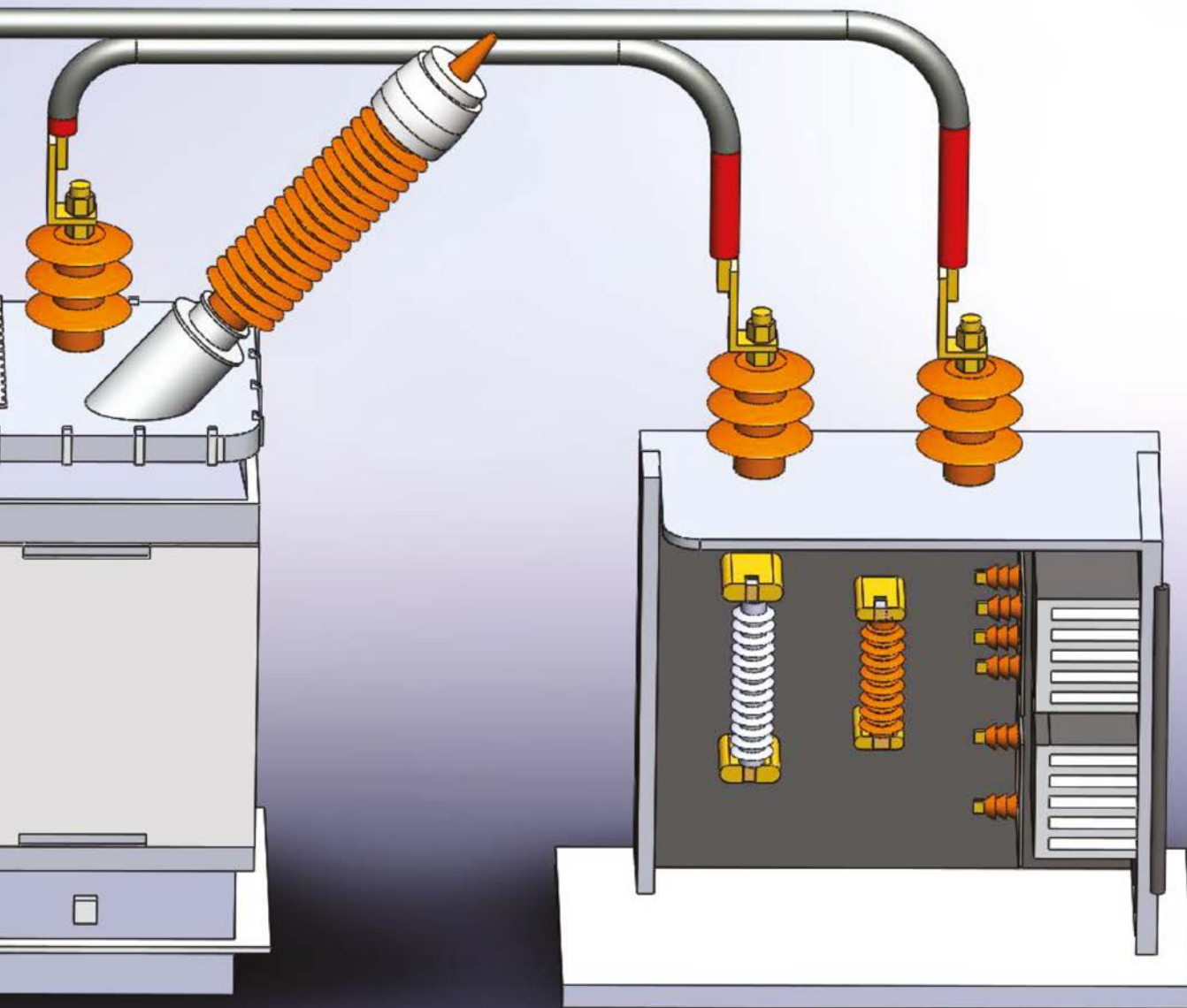


Due to the development of modern grids and the extensive implementation of distributed generators, the fault current level increases, which affects the operation of circuit breakers



Impact of controllable superconducting series reactor in transient recovery voltage of circuit breaker

How can a controllable superconducting series reactor suppress transient recovery voltage of a circuit breaker?



1. Introduction

Due to the development of modern grids and the extensive implementation of distributed generators, the fault current level increases, which affects the operation of circuit breakers (CB) [1]. Transient recovery voltage (TRV) is a concern that can damage a CB [2]. Saving a CB from failure needs special attention to both current

fault level and TRV factors based on IEEE Std C37.119-2016 [3].

The most common solution to protect the CB from fault current is either magnetic-based [4] or resistive-based [5]-[7] superconducting fault current limiters. Among different types of superconducting fault current limiters (SFCL). Among

types of superconducting FCLs, the inductive SFCL is a piece of protection equipment that limits the fault current by imposing inductance to faulty lines [8]-[9]. Its inductance is very low in the normal state of the power system [10]. An SFCL can be very useful for protecting the CB from raising the fault current level [11].

ABSTRACT

Series reactors as fault current limiters (FCLs) are extensively employed to enhance power grid protection issues. Utilizing superconducting technology is a viable solution to approach FCLs toward commercializing. The concern of transient recovery voltage (TRV) of the circuit breaker becomes more

considerable due to FCL's high stored energy in the case of fault current limiting mode. This paper firstly focuses on the analysis of TRV under the presence of an inductive-based superconducting fault current limiter (SFCL) installed in a power grid, and then it investigates the impact of a controllable superconducting series reactor (CSSR) in TRV of the circuit breaker.

The obtained results show that the synchronous operation of a CSSR with a circuit breaker substantially declines TRV.

KEYWORDS:

circuit breaker, fault current limiter, superconducting series reactor, transient recovery voltage

By opening a line that has the short circuit fault due to the high stored energy in series inductors, the voltage of the opened CB rises, which can cause problems and damage

The next important matter for CB operation is the occurrence of the CB terminal TRV. This phenomenon depends on equivalent inductance, resistance, and capacitance of the faulty system [12]. Moreover, the inductance of a faulty electric system with the presence of SFCL increases, which affects the factors of TRV as the peak of TRV, frequency, rate of raising recovery voltage (RRRV), and TRV damping constant [13].

In this paper, TRV of CB is investigated, whereas SFCL is not employed. Then, the TRV of the circuit breaker is discussed, considering the inductive SFCL in series with the faulty line. Next, the behavior of the controllable superconducting series reactor (CSSR) as a TRV reduction circuit is described. It is shown that not only is this topology able to limit the magnitude of TRV, but it also can protect the CB from the sharp raising of recovery voltage. The contributions of this work are as follows:

- an overview of the inductive SFCL effect in TRV of a circuit breaker
- effect of a CSSR in TRV of a circuit breaker

- finite element based magnetic field analysis and transient simulation of the proposed CSSR

This paper is prepared as follows: section 2 compares the TRV of a CB with and without an SFCL, section 3 discusses the configuration of the proposed CSSR, and in the next section operation, and effects of the CSSR in TRV of the circuit breaker are discussed. In section 5 superconducting reactor is simulated by magnetic FEM, and in section 6, the achievements of the CSSR are explained, and finally, a conclusion is given.

2. Study of TRV of the CB in the presence of an SFCL

In this section, the effect of TRV of a CB under short circuit conditions is investigated. The power line faced a high current while a small impedance is connected to the electrical system which is known as a short circuit fault. In this case, the CB is activated as protection equipment to save the power system from severe damage. By opening a faulty line, due to high stored energy in series inductors, the opened CB

voltage is moderately raised. Fig. 1 depicts a model of an electrical system with and without the inductive SFCL in the fault condition.

As shown in Fig. 1(a), the equivalent circuit is assumed where there is no inductive SFCL installed in the faulty line. Additionally, the upstream grid Thevenin voltage is modeled as voltage source V_{th} and, the whole series inductance and resistance of the electrical system are modeled as Z_{eq} , respectively. In this figure, C_{CB} is the shunt capacitance model of the CB in the open position. The depicted equivalent circuit in Fig. 1(b) is similar to the equivalent circuit in Fig. 1(a), except that this equivalent circuit also includes an SFCL. In the following sections, based on the explained equivalent circuits, the TRV of the circuit breaker is analytically studied and simulated. These RLC circuits are valid to analyze the TRV of the CB based on IEEE C37.011-2011.

2.1 TRV of the CB without installing an SFCL

According to the equivalent circuit of Fig. 1(a), by applying Kirchhoff voltage law, equations 1 and 3 can be calculated as:

$$TRV = V_{CB} = -\frac{1}{C_{C.B}} \int i_f(t) dt = -v_{th}(t) + R_{eq}(i_f(t)) + L \frac{di_f(t)}{dt} \tag{1}$$

upstream grid voltage $V_{th}(t)$ is defined as:

$$v_{th}(t) = V_m \cos \omega t \tag{2}$$

Where V_m is the maximum amplitude of voltage, t is the time domain, R_{eq} and L_{eq} are the equivalent resistance and inductance of the grid. By solving equation 1 and considering some of the approximation, the CB's voltage in the open position as TRV is expressed as equation 3.

$$TRV = V_{CB} = -\frac{\omega_0^2}{\omega_0^2 - \omega^2} V_m (\cos \omega t - ke^{-\alpha t} \cos \omega_0 t) \tag{3}$$

$$\omega_0 = \frac{1}{\sqrt{L_{eq} C_{C.B}}} \tag{4}$$

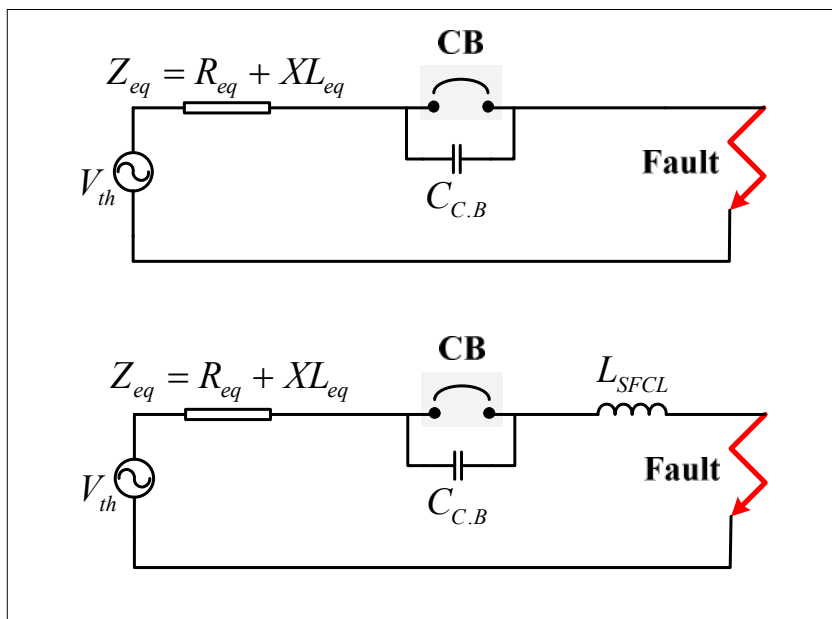


Figure 1. Equivalent circuit of a faulty line with and without an inductive SFCL

$$\omega = 2\pi f \quad (5)$$

$$f_0 = \frac{\omega_0}{2\pi} \quad (6)$$

$$\alpha = \frac{R_{eq}}{2L_{eq}} \quad (7)$$

where ω is the grid angular velocity, ω_0 is the TRV radius velocity, α is the damping coefficient, and k is a coefficient that depends on the initial value of the circuit. It is obtained from equation 3 that the TRV peak value depends on the value of ω_0 and dependently L_{eq} and C_{CB} , and coefficient k as depicts in equation 4, whereas the constant damping time depends on the ratio of R_{eq} to L_{eq} according to equation 7.

The rate of raising recovery voltage (RRRV) is a significant factor that can be calculated from TRV of the CB according to equation 8. This factor depends on the first peak of TRV, and its oscillation

frequency of the RLC modeled circuit as presented in IEC 62271-101.

$$RRRV = \frac{TRV_{peak}}{1 / 2f_0} \quad (8)$$

In the first step of simulations, TRV of the CB was investigated without using an inductive SFCL as a protective series reactor. As shown in Fig. 2, it is clear that the peak value of TRV of the CB experiences 115 kV, while TRV damping duration is almost 200 ms, and its amplitude reaches to grid voltage equal to 63 kV. In Fig. 2, as shown in the enlarged time duration 426-446 ms, the TRV frequency can be obtained in the time domain between 0.43-

0.44 ms, which is approximately 3500 Hz. In this case, RRRV is 821 kV/ms.

2.2. TRV of the CB with installing an inductive SFCL

According to the equivalent circuit in Fig. 1(b), by employing an inductive SFCL, the inductance of the system is substantially increased compared to the equivalent circuit in Fig. 1(a), which does not have an SFCL. As a result of the increase of the inductance value, the TRV radius velocity is declined. Meanwhile, the damping duration is considerably raised. Besides, the TRV peak value is fallen as a result of decreasing the line current initial value.

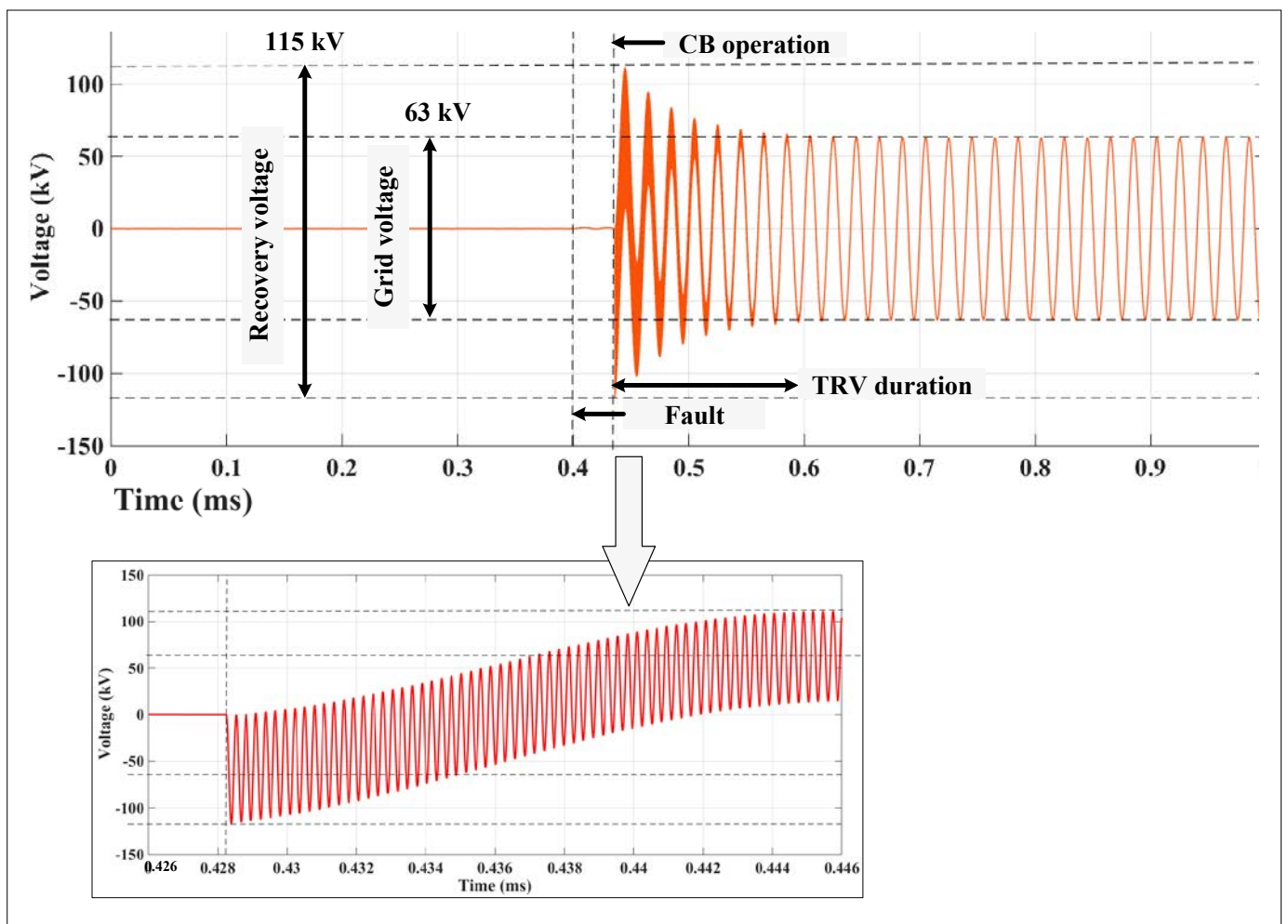


Figure 2. TRV of circuit breaker without installing inductive SFCL

$$\omega_0 = \frac{1}{\sqrt{(L_{eq} + L_{SFCL}) C_{C.B}}} \quad (9)$$

$$\alpha = \frac{R_{eq}}{2(L_{eq} + L_{SFCL})} \quad (10)$$

where L_{SFCL} is SFCL the inductance. To calculate the TRV of the CB by the presence of an inductive SFCL, equation 3 must be utilized by considering 9 and 10.

In the second step of the simulations, the TRV of the CB is concentrated consider-

ing the installed inductive SFCL. In Fig. 3 it is demonstrated that the magnitude of TRV of the CB is reached 82 kV, once damping time is increased, and voltage magnitude steadily reaches to 63 kV. The obtained results show that the TRV frequency is limited to 550 Hz and, RRRV is decreased to 41 kV/ms.

To briefly sum up obtained results from this section, Table 1 is given to compare the effects of an inductive SFCL in TRV of the CB. It is extracted from Table 1 that using an SFCL decreases: TVR peak value up to 29%, TVR frequency up to 86%, and 95% of RRRV while it increases up to 86% of TRV damping time. Damping constant

raising causes slow CB operation, which is not acceptable.

3. Configuration of the proposed CSSR

In this section, the configuration of the proposed CSSR and its operation are discussed. Fig. 4(a) illustrates the installed CSSR is in series with the circuit breaker. The proposed CSSR structure comprises a superconducting coupled reactor, solid-state switches, includes four diodes and IGBT, and a parallel resistor-arrester damper circuit. In this diagram, it is considered that fault likely to happen downstream. Fig. 4(b) depicts different sections of the proposed CSSR.

3.1 Specification of the series reactor and its modeling

In the term of CSSR operation, the series reactor (SR) is designed based on a superconducting structure in both normal and fault states. This reactor is prepared using liquid nitrogen cooling system at 77 K,

The proposed CSSR structure comprises a superconducting coupled reactor, solid-state switches, which includes four diodes and IGBT, and a parallel resistor-arrester damper circuit

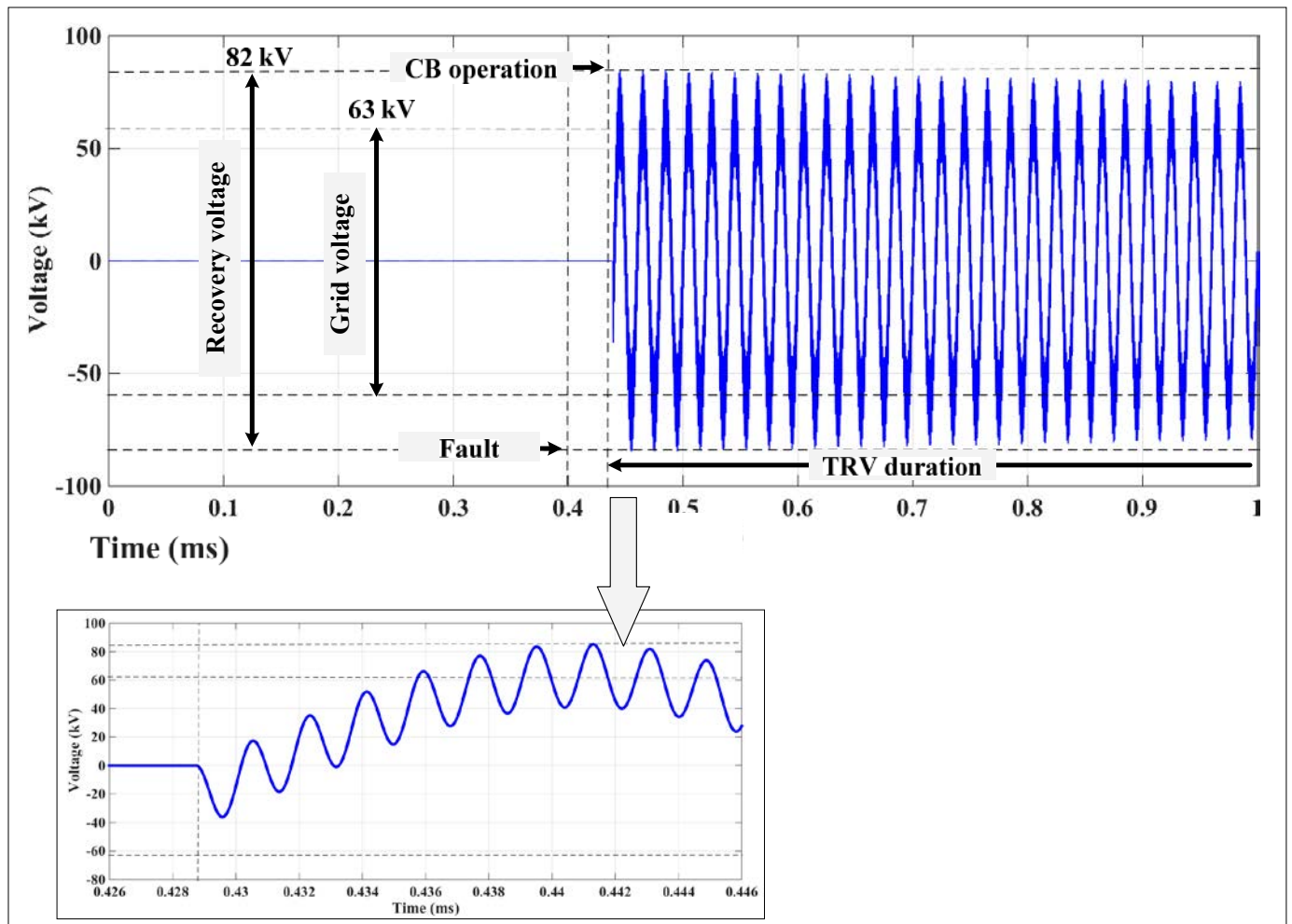


Figure 3. TRV of the circuit breaker with installing an inductive SFCL

The controllable current series reactor uses a liquid nitrogen cooling system at 77 K, superconducting wire type Bi-2223 and a ferromagnetic steel iron core

Table 1. Comparison of TRV in power line with and without the presence of an inductive SFCL

Compared factor	Protected line by SFCL	Unprotected line
Peak of TRV	82 kV	115 kV
TRV damping time	1500 ms	200 ms
TRV frequency	550 Hz	3500 Hz
RRRV	41 kV/ms	821 kV/ms

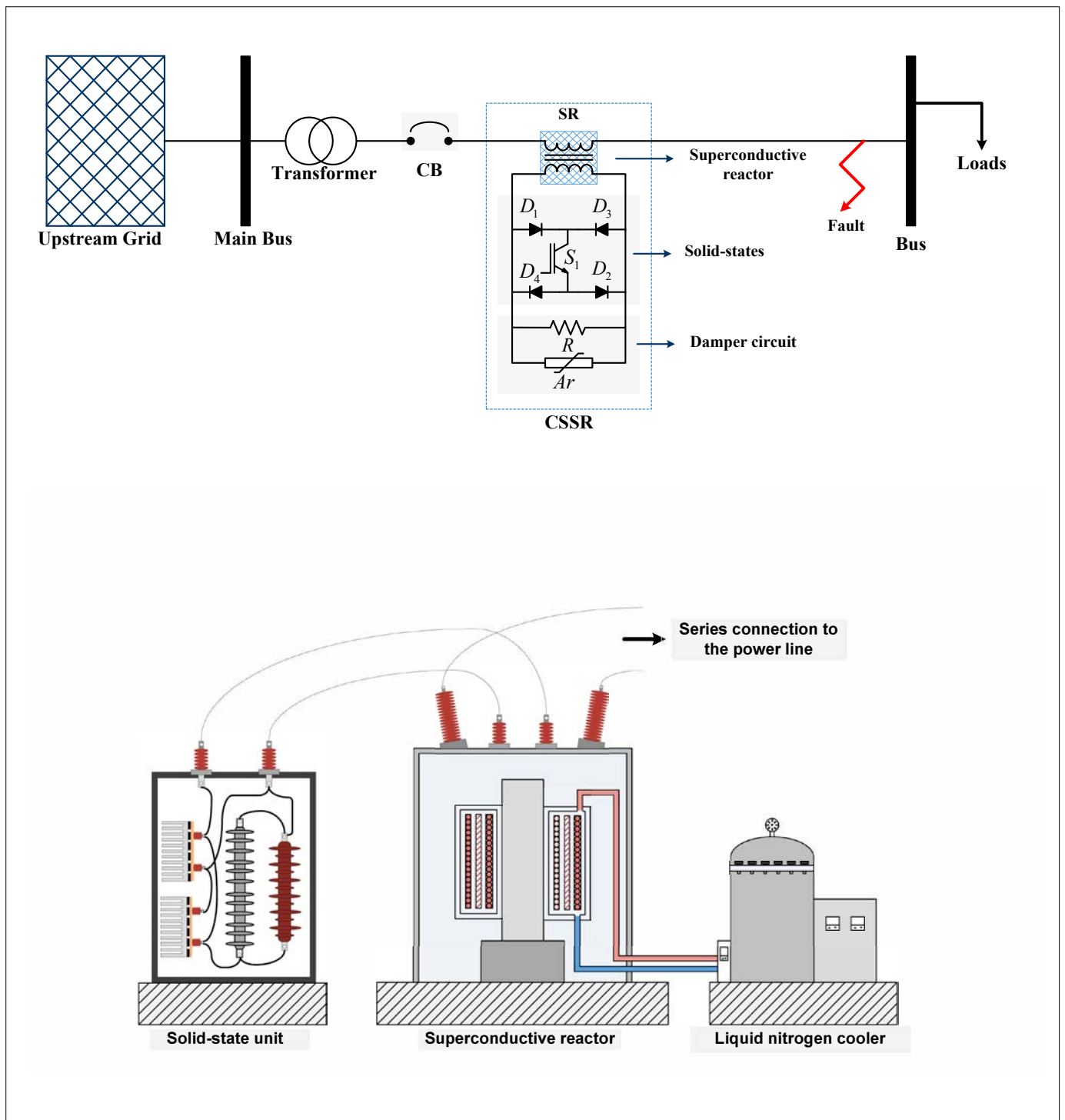


Table 2. Features of superconducting wire and the cooler

Feature	Discretion
wire code	Bi-2223
type	Ag-sheathed tap HT-CA
material	Cu alloy
critical current	1500-1700
width	16 mm
thickness	1.2 mm
cooler system	liquid nitrogen
cooling mechanism	gas condensation
reservoir tank	200 liter
temperature	77 K

In the normal operating state, the CSSR has its minimum inductance and transfers electric power from the grid side to the load side, with the minimum voltage drop

Bi-2223 wire and ferromagnetic steel iron core. Specification of a superconducting wire and the cooling system is presented in Table 2.

According to Fig. 5, the primary winding current results in a magnetic flux that is called φ_p , also the secondary current generates a flux φ_s that is in the reverse direction of primary flux. Subtracting these two magnetic flux values from each other results in the main core flux. Fig. 6 demonstrates the core magnetic flux and its electrical equivalent circuit.

Considering the equivalent circuit in Fig. 13, the main arm magnetic link flux is calculated by equation 11.

$$\varphi_l = \varphi_p - \varphi_s = \frac{(N_p i_f) - (N_s i_s)}{R_m + \left(\frac{R_{s1} \cdot R_{s2}}{R_{s1} + R_{s2}}\right)} \quad (11)$$

$$\varphi_{pl} = \frac{(N_p i_f)}{R_{a1}}, \varphi_{sl} = \frac{(N_s i_s)}{R_{a2}} \quad (12)$$

$$V_p = \frac{(di_f)}{R_{a1} dt} + N_p \frac{(N_p di_f/dt) - (N_s i_s/dt)}{R_m + \left(\frac{R_{s1} \cdot R_{s2}}{R_{s1} + R_{s2}}\right)} \quad (13)$$

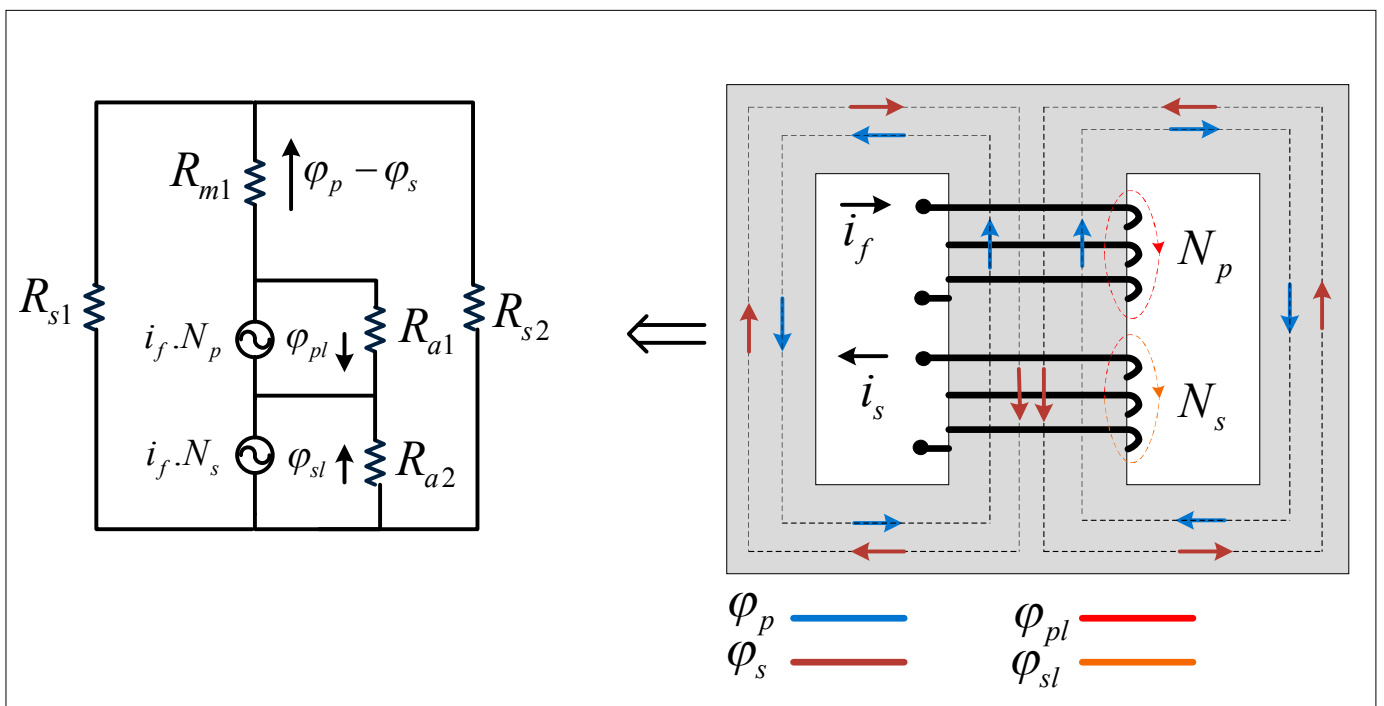


Figure 5. Magnetic structure of CSSR and its electric equivalence circuit

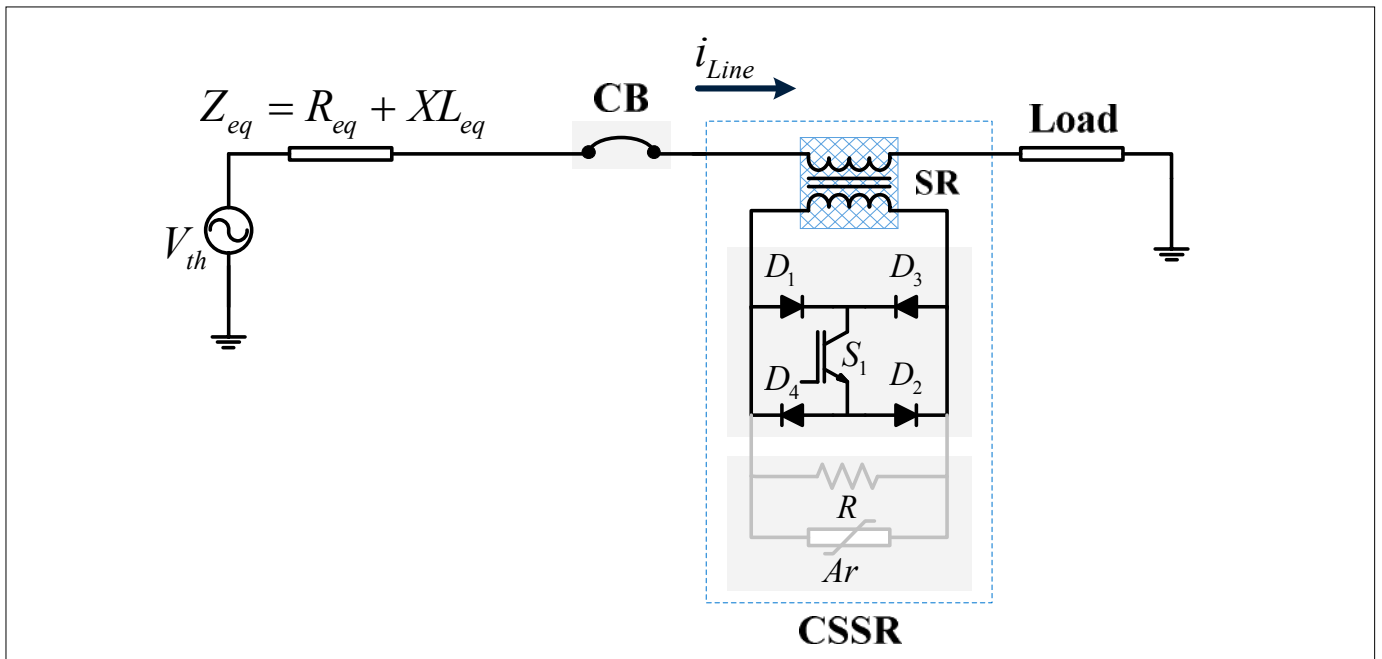


Figure 6. CSSR operation in the normal state when S_1 is turned on

Here, i_f and i_s are current of the primary and secondary winding. N_p and N_s are primary and secondary winding turn numbers, beside φ_{pl} and φ_{sl} are their leakage flux, respectively. In addition, R_m , R_{s1} , R_{s2} are the main and side arms reluctance. Furthermore, R_{a1} and R_{a2} are the leakage flux air path reluctance. Equation 10 express link flux in the main arm, and 12 define the value of leakage flux for both windings. Also, equation 13 shows the primary winding voltage, which effectively influences the TRV of the CB.

3.2 Solid-state section of CSSR

The solid-state section consists of four diodes D_1 - D_4 and an IGBT switch. In the normal state, the IGBT gate is derived by logic pulse, and the alternate current of the secondary winding reactor is conducted by diodes and turned-on IGBT. At the same

time, the circuit breaker is closed to transfer power from upstream to load sections. In the fault event, a trip is sent to both CB and CSSR, synchronously. Therefore, the IGBT of CSSR is turned off once the CB begins to break. At this moment, the resistance R and arrester Ar current rise to damp dissipation energy of the circuit and suppress IGBT voltage. As a result of solid-state circuit operation, the SR magnetic flux is moderately increased while SR reverse inductive voltage suppresses the TRV of the CB.

4. Operation of CSSR

In this section, the CSSR functional specification is discussed in the normal operation and fault state, and its ability is analysed and simulated to reduce the TRV of the CB. The obtained results confirm the feasible operation of the proposed CSSR to reduce TRV of the CB.

4.1 CSSR operation in normal state

In the normal state, the CSSR has its minimum inductance and transfers electric power from the grid side to the load side, with the minimum voltage drop. This function is performed by solid-state switches in the secondary side of the superconducting reactor, whereas D_1 , D_2 , and S_1 conduct a positive cycle of secondary current, beside D_3 , D_4 , and S_1 conduct a negative cycle of secondary current. Fig. 6 illustrates the proposed CSSR in a normal state.

According to Fig. 6, for CSSR operation in a normal state by operating the solid-state as AC switch, the secondary of the superconducting reactor is bypassed. For the analytical study of this operation, the T-model of the reactor is considered, as shown in Fig. 7.

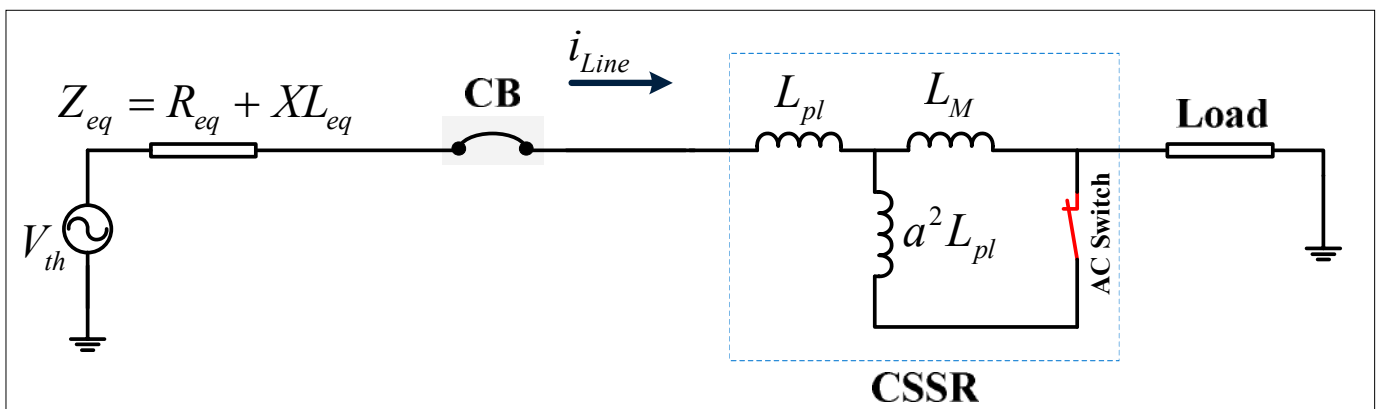


Figure 7. CSSR T-model in the normal state when S_1 is turned on

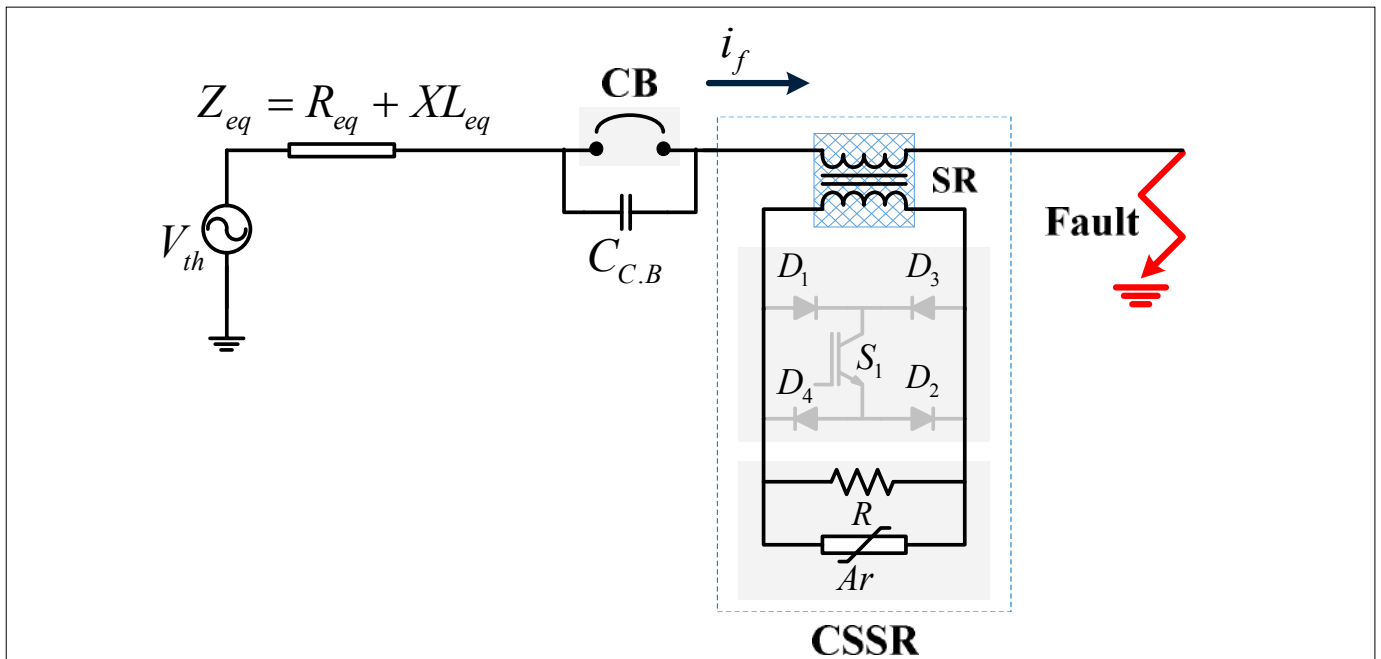


Figure 8. CSSR operation in fault state when S_1 is turned off

The simulation results demonstrate that the magnitude of TRV of the CB reaches 70 kV, while TRV damping time is limited to 20 ms, which proves the effectiveness of the presence of a CSSR in the grid

The CSSR T-model in the normal state depicted in Fig. 6, L_{pl} and L_{sl} are leakage inductance of the superconducting inductance, and L_M is magnetization inductance of the reactor. By closing the solid-state switch S_1 , the CSSR inductance substantially falls. Equation 14 defines the line's current in a normal state.

$$I_{line} = \frac{V_{th}}{R_{eq} + j\omega(L_{eq} + L_{pl} + a^2 L_{sl}) + Z_{load}} \quad (14)$$

Here, Z_{load} is the load impedance. The CSSR leakage inductance value is much lower than the equivalent system inductance, which can be neglected. Therefore, the CSSR voltage drop in the normal state is negligible.

4.2 CSSR operation in the fault state

Fig. 8 illustrates a diagram of the power system when the fault occurs in the downstream power line. A trip command is sent to both the CB and IGBT S_1 syn-

chronously in this state of operation. As a result of the controlling command, the CB opened, and in addition, S_1 is turned off to suppress TRV of the CB. By opening the S_1 , the current of the secondary is commutated into the arrester A_r and resistor R . In this state of operation, A_r saved solid-state switches from voltage stress and R damps transient behavior of the system.

As depicted in Fig. 9, in a fault state to CSSR behavior clarify, a superconducting reactor T-model is used.

According to the CSSR T-model in a fault state, when S_1 is turned off, the inductance and resistance of the electric system considerably rise. This increase in inductance and resistance is due to a series connection between a parallel branch consisting of L_M and $a^2 R$ with the faulty line. To simplify the CSSR model, the L_{pl} and L_{sl} values are

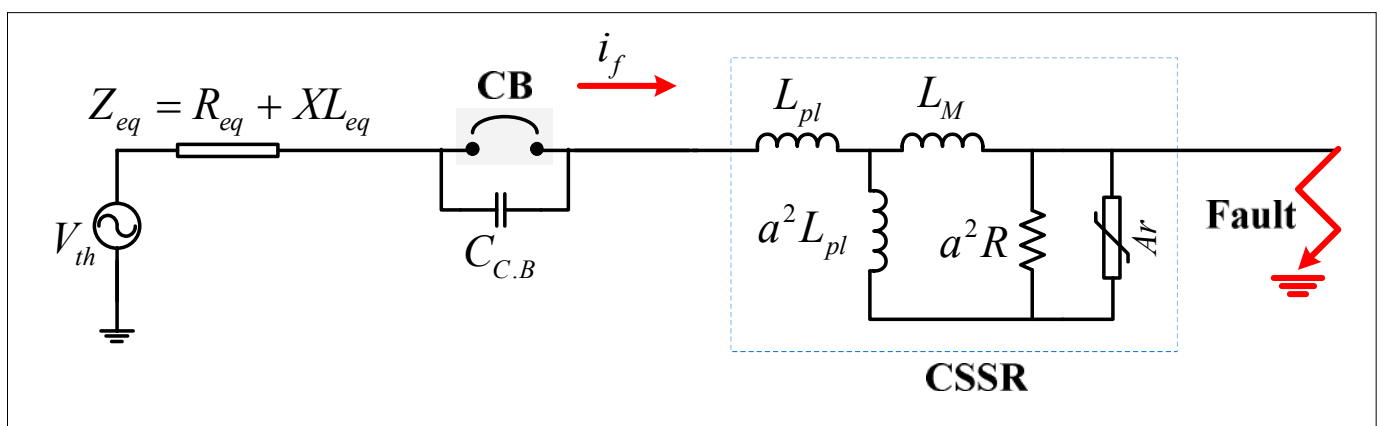


Figure 9. CSSR T-model in fault state when S_1 is turned off

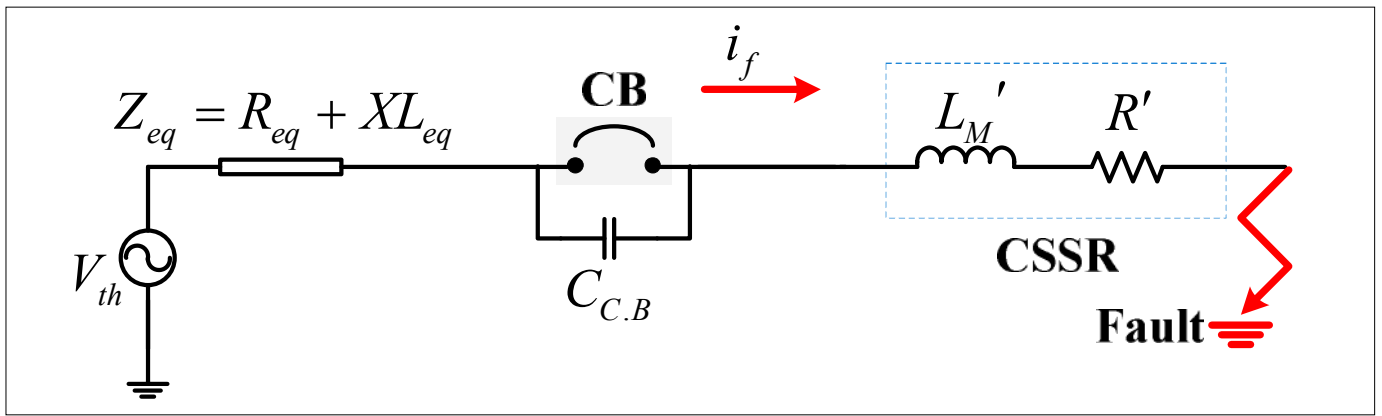


Figure 10. Approximate model of the CSSR in fault state when S₁ is turned off

ignored. On the other hand, A_r's operation is in the short period of first voltage stress so that it can be removed from the final model. Consequently, the only remained

elements are parallel magnetization inductance and secondary connected resistor. In Fig. 8, based on the Thevenin model, the CSSR series is depicted.

In this state, the TRV of the CB is explained by equation 15, which is confirmed by the simulation result in Fig. 10.

$$TRV = V_{C.B} = - \frac{\frac{V_*}{(L_{eq} + L_M') C_{C.B}}}{\frac{1}{(L_{eq} + L_M') C_{C.B}} - (2\pi f)^2} \left(\cos(2\pi ft) - ke^{-\frac{R_{eq} + R'}{2(L_{eq} + L_M')} t} \cos\left(\frac{t}{(L_{eq} + L_M') C_{C.B}}\right) \right) \quad (15)$$

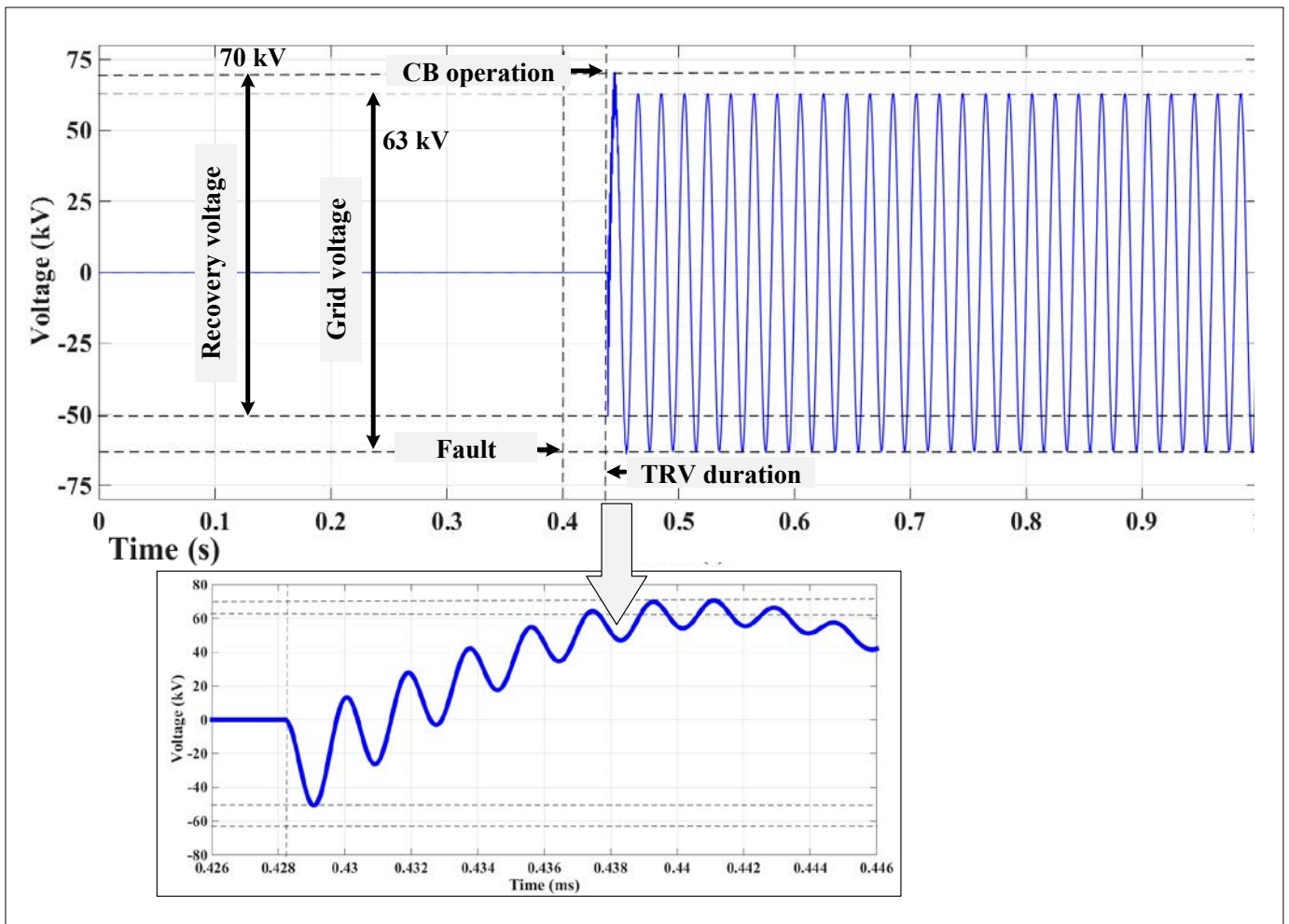


Figure 11. TRV of CB with installing CSSR

The magnetic field distribution of the proposed superconducting reactor is investigated using the electromagnetic 3D FEM model with the ANSYS Maxwell software

As depicted in Fig. 7, the simulation results prove the effectiveness of the presence of a CSSR in the grid. In Fig. 11, TRV of the CB is demonstrated when a fault occurs in 0.43 s. In this figure, is demonstrated that the magnitude of TRV of the CB reaches 70 kV, while TRV damping time is limited to 20 ms. The

obtained results show that the TRV frequency is limited to 400 Hz, and RRRV is decreased to 28 kV/ms.

4.3 CSSR power loss calculation

In this section, the power loss of the proposed CSSR is briefly described in both

normal and fault state. In the normal state, total power loss consists of superconducting wire (Bi-2223) AC power loss [14] in primary and secondary coils, IGBT power loss, and diodes power loss. In the fault condition, total power loss consists of superconducting wires, AC power loss, and damper resistor power loss.

5. Magnetic study of the proposed CSSR

Because of the inherent non-linear magnetic characteristics of the proposed superconducting reactor, numerical methods must be used for the calculation of the

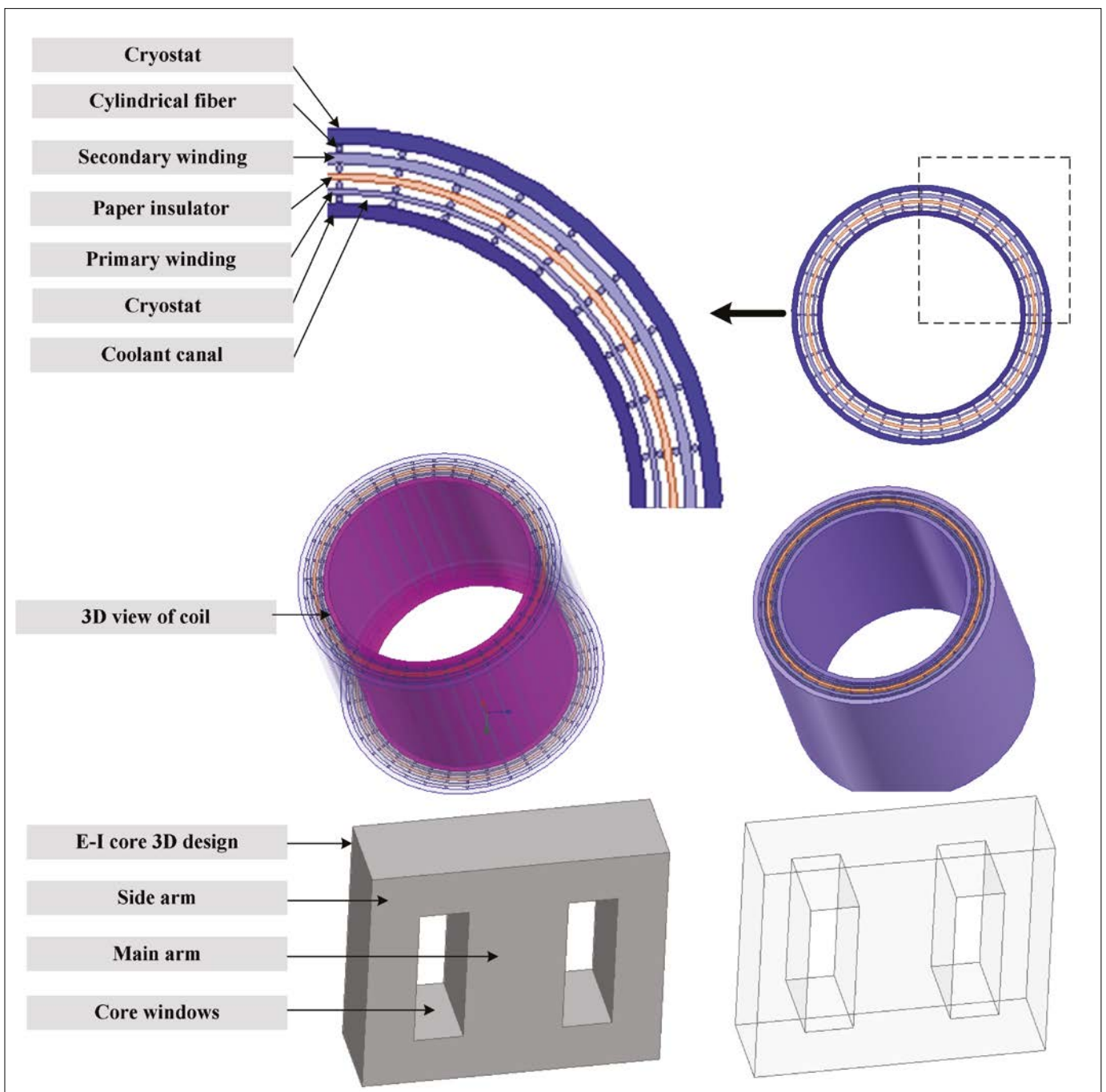


Figure 12. Geometric view of series reactor sections

magnetic field distribution and the prediction of the magnetization characteristics. The Finite Element Method (FEM) is a well-known numerical method for field solution and design validation of electromagnetic structures with complex geometry and non-linear properties. In this section, the magnetic field distribution of the proposed superconducting reactor is investigated considering the 3D FEM model utilizing the ANSYS Maxwell software. The solver is A-Phi transient, and length-based mesh is applied in simulated sections. The designed geometric scheme of the proposed superconducting reactor is shown in Fig. 12.

5.1 Geometric of the proposed CSSR

Fig. 11(a) shows that the coil is comprised of a superconducting cooling system box

as a thermo-isolator, a primary winding and a secondary winding, an electric paper sheet insulator, separator cylindrical fibre insulation. On the other hand, the CSSR core material is magnetic steel iron that is designed in an E-I manner, as illustrated in Fig. 11(b).

Fig. 13 depicts 2D and 3D views of the reactor in which the ferromagnetic core and the designed coil have been assembled,

whereas the coil is placed around the core main arm.

5.2 Magnetic FEM simulation of CSSR

In this step, the length-based meshes are applied in the 3D geometric scheme of the superconducting reactor considering optimized length-based mesh operation. The mesh plot is exhibited in Fig. 14.

The numerical 3D FEM simulation results confirm that the CSSR can impose an acceptable inductance value to the faulty line, and its voltage drop suppresses the TRV of the CB to the acceptable value

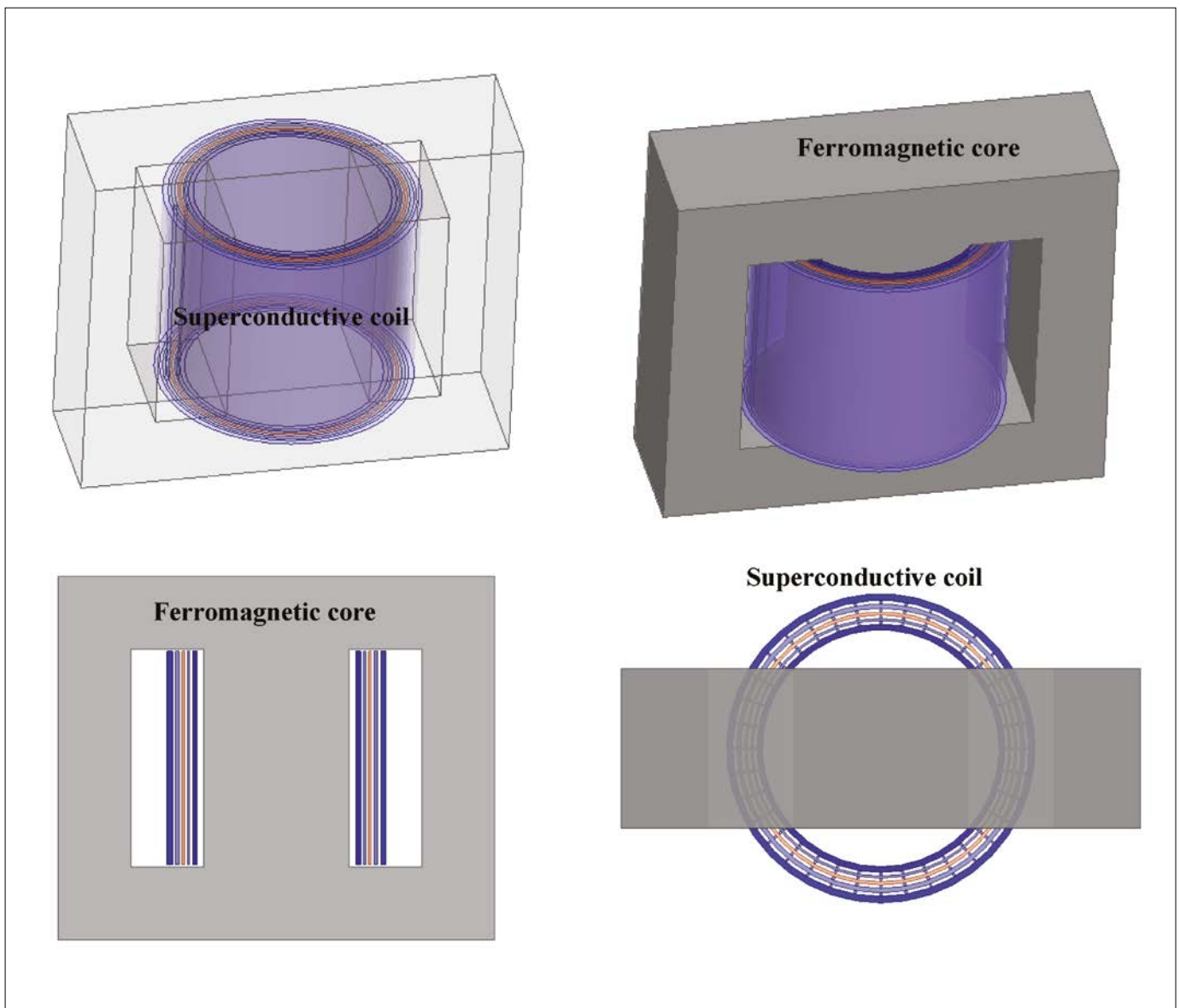


Figure 13. 2D and 3D illustration of an assembled series reactor

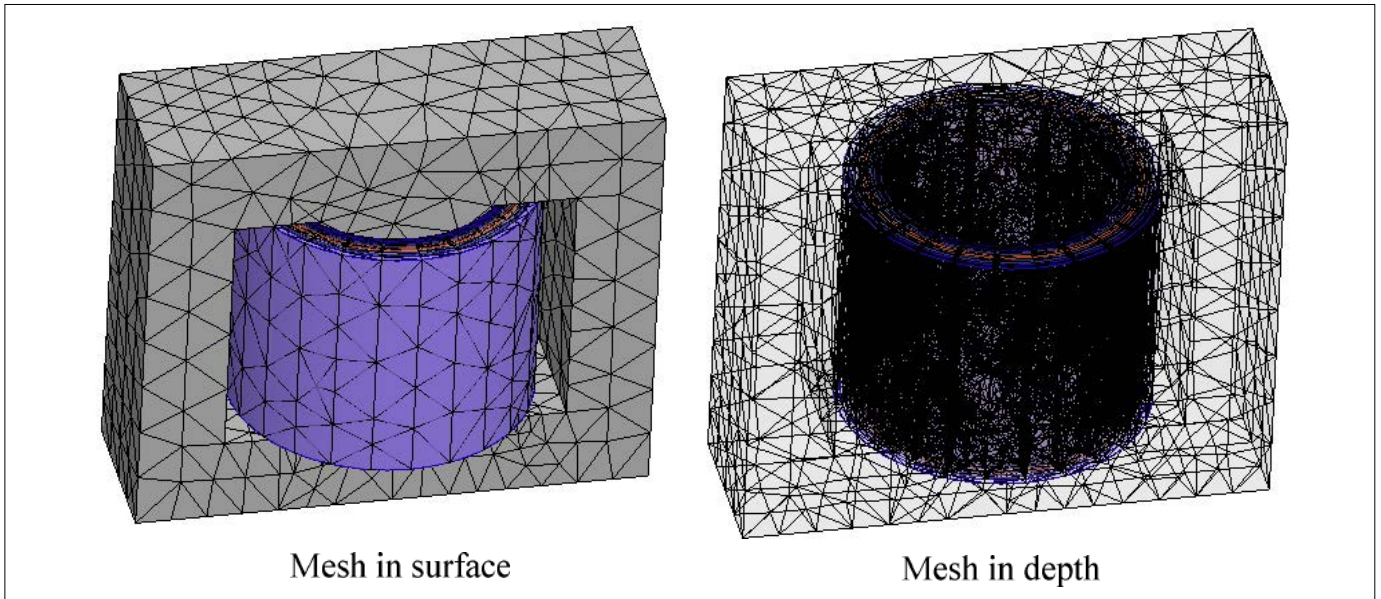


Figure 14. Mesh operation of the series reactor

In this step of the simulation, the focus is on the core magnetic field analysis, considering a normal operation, in which the AC switch bypasses the secondary coil, and the line current passes through the primary winding. In Fig. 15 transient FEM analysis result is presented. As shown in this figure, to increase the simulation result visibility, 2D and 3D

views are presented together. Vector and magnitude distribution of the magnetic flux are illustrated, while the main arm average flux does not exceed 1.7 mT. The obtained results from the FEM simulation confirm that, in the normal operation, the imposed CSSR series inductance is substantially low. Therefore, the CSSR series voltage drop is small.

In the ultimate FEM simulation step, it is considered that the AC switch in the secondary side is opened, and the secondary winding current is limited by the commutated current into resistor R. In Fig. 16 is depicted that the main arm average magnetic flux density reaches 1.1 T as its maximum value, whereas the magnetic flux density in the saturation is 1.8 T. The

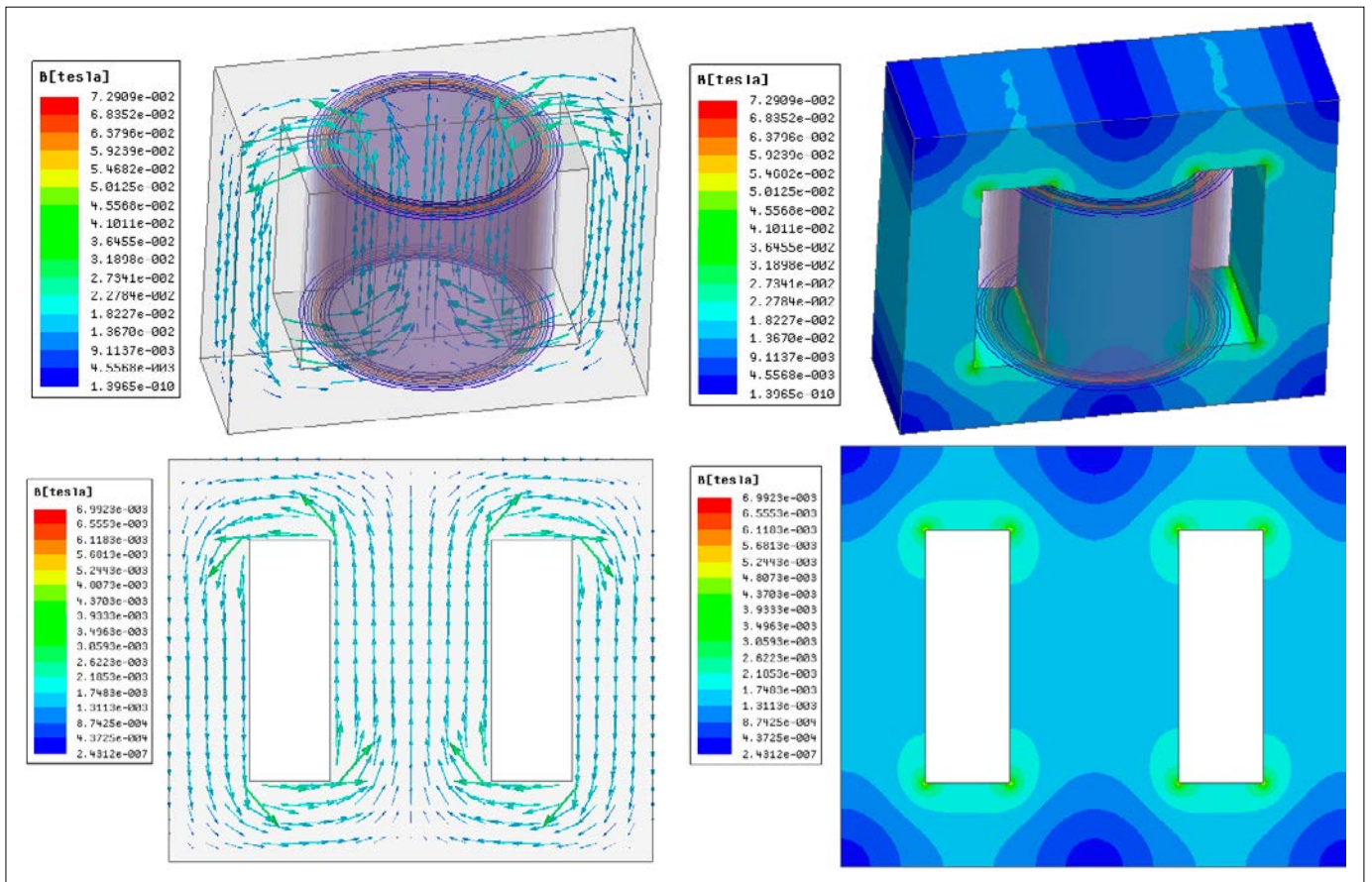


Figure 15. 2D and 3D magnetic flux density of series reactor (normal state)

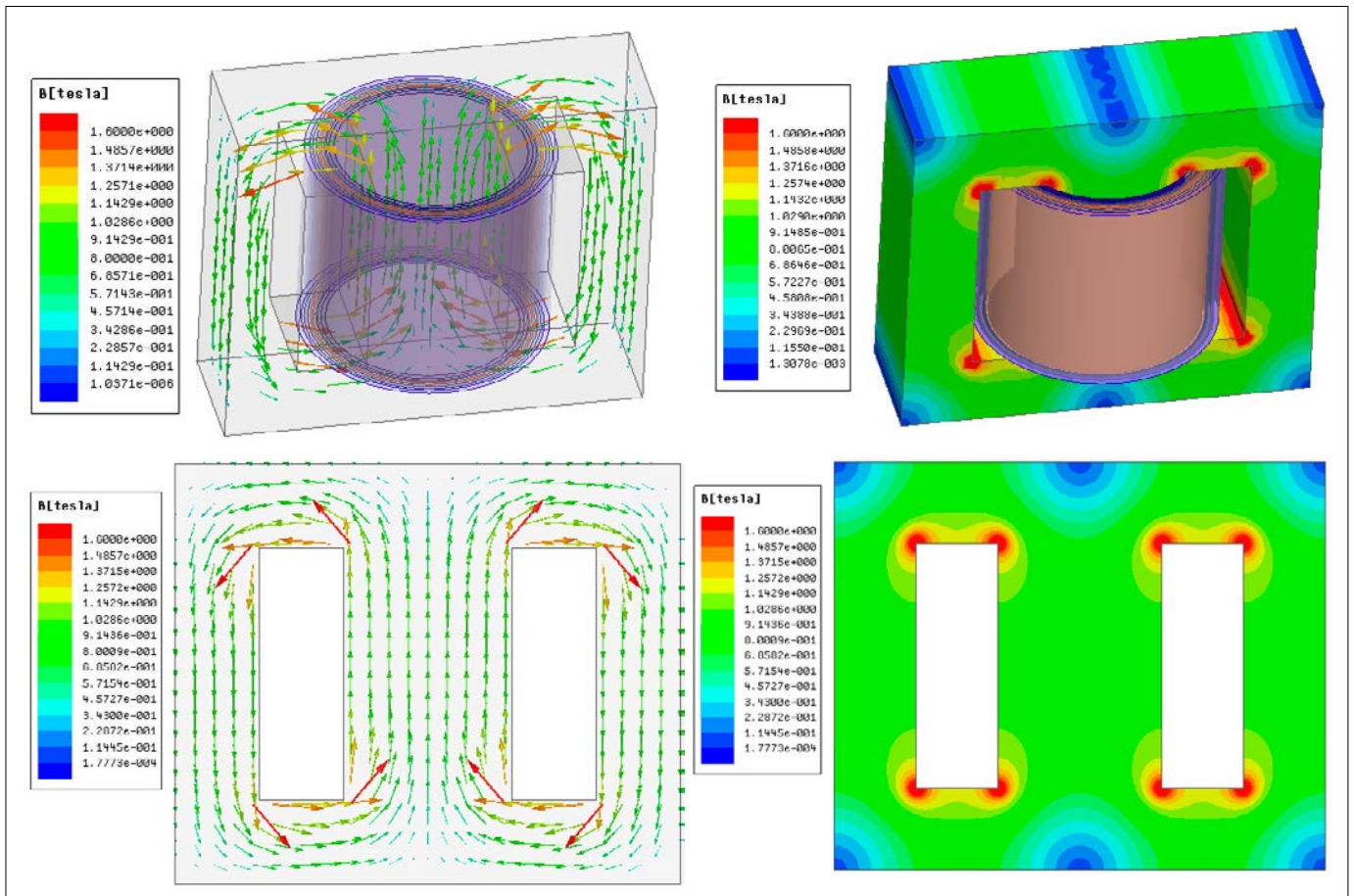


Figure 16. 2D and 3D magnetic flux density of series reactor (fault state)

simulation results confirm that the CSSR can impose an acceptable inductance value to the faulty line, and its voltage drop suppresses the TRV of the CB to the acceptable value.

6. The CSSR features in the TRV of CB

In this paper, the effects of the SFCL and the proposed CSSR on the TRV of the CB are investigated. To describe the benefits of employing the proposed CSSR, a comparison of TRV of the CB with the effects of an inductive SFCL and CSSR is presented in Table 3.

It is defined in Table 2 that using the CSSR provides more release in comparison with the SFCL as there is a decrease in the TVR peak value up to 15 %, TVR frequency up to 28 %, and 32 % of RRRV once it reduces 98.5 % of TRV damping time. Fig. 17 shows the CB's TRV plot with both SFCL and CSSR.

In Fig. 17, it is obvious that the damping of the TRV is significantly faster when the CSSR is used, compared to the steadily damping of the TRV when the SFCL is

Table 3. Comparison of TRV of the CB with effects of an inductive SFCL and CSSR

Compared factor	Protected line by CSSR	Protected line by SFCL
Peak of TRV	70 kV	82 kV
TRV damping time	20 ms	1500 ms
TRV frequency	400 Hz	550 Hz
RRRV	28 kV/ms	41 kV/ms

used. Also, it shows the TRV peak value has declined by 12 kV.

It is understood that the functional effects of the CSSR cause the extensive improvements in TRV of the CB as follows:

- decreasing peak value of TRV up to 15 %
- decreasing TRV frequency up to 28 %
- decreasing RRRV up to 32 %
- decreasing duration of TRV damping up to 98.5 %
- low power loss because of superconductivity.

In future research, it can be proved that not only the proposed CSSR can relieve the TRV factor, but also it can solve other matters depending on system overvoltages, as follows:

- damping ferroresonance of voltage transformer
- damping ferroresonance of power transformer
- damping transient voltage fluctuation in power system
- limiting current overshoots in load variation.

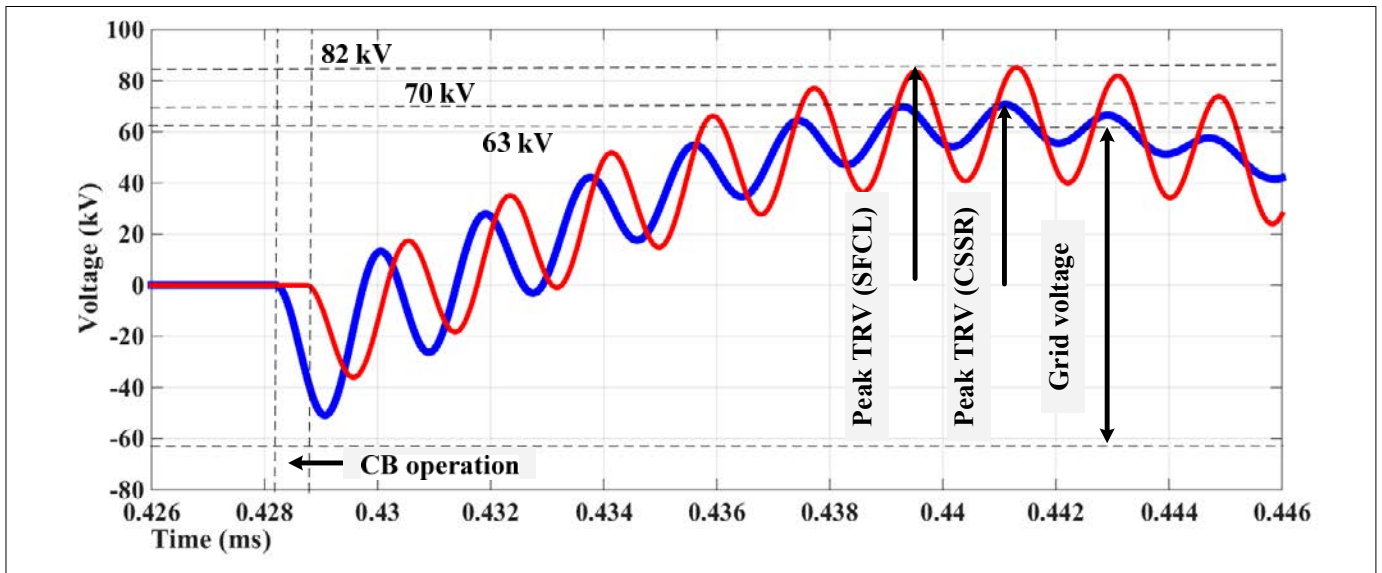


Figure 17. TRV signal comparison with the effect of an inductive SCFCL and CSSR

The primary CSSR implementation scheme, as illustrated in Fig. 18, has been developed considering all required sections for CSSR development. It serves for future planning and implementation.

Conclusion

The issue of power system protection against fault current directly depends on the operation of fault current limiters and circuit breakers. One of the most significant factors which influence the normal behavior of circuit breaker and its features is transient recovery voltage which can extensively damage circuit breaker. In this paper, first of all, the transient recovery

voltage of the circuit breaker is investigated without installing the superconducting fault current limiter, and then the installation of the inductive superconducting fault current limiter was investigated. The primary results show that inductive superconducting fault current limiter can limit the peak value of transient recovery voltage. In addition, it can limit the frequency of transient recovery voltage and its rate of raising recover voltage. However, it substantially increases the TRV damping time constant. In the second step, the operation of the proposed controllable superconducting series reactor was investigated. Indeed, the controllable superconducting series reactor showed excellent

performance regarding all the harmful factors of transient recovery voltage as its peak value, frequency, rate of raising recovery voltage, and damping time constant. Consequently, the implementation of the controllable superconducting series reactor can entirely save circuit breakers in the power system.

Bibliography

- [1] H. Radmanesh, S. H. Fathi, G. B. Gharehpetian, A. Heidary, *A novel solid-state fault current-limiting circuit breaker for medium-voltage network applications*, IEEE Transactions on Power Delivery, Vol. 31, No. 1, 2016

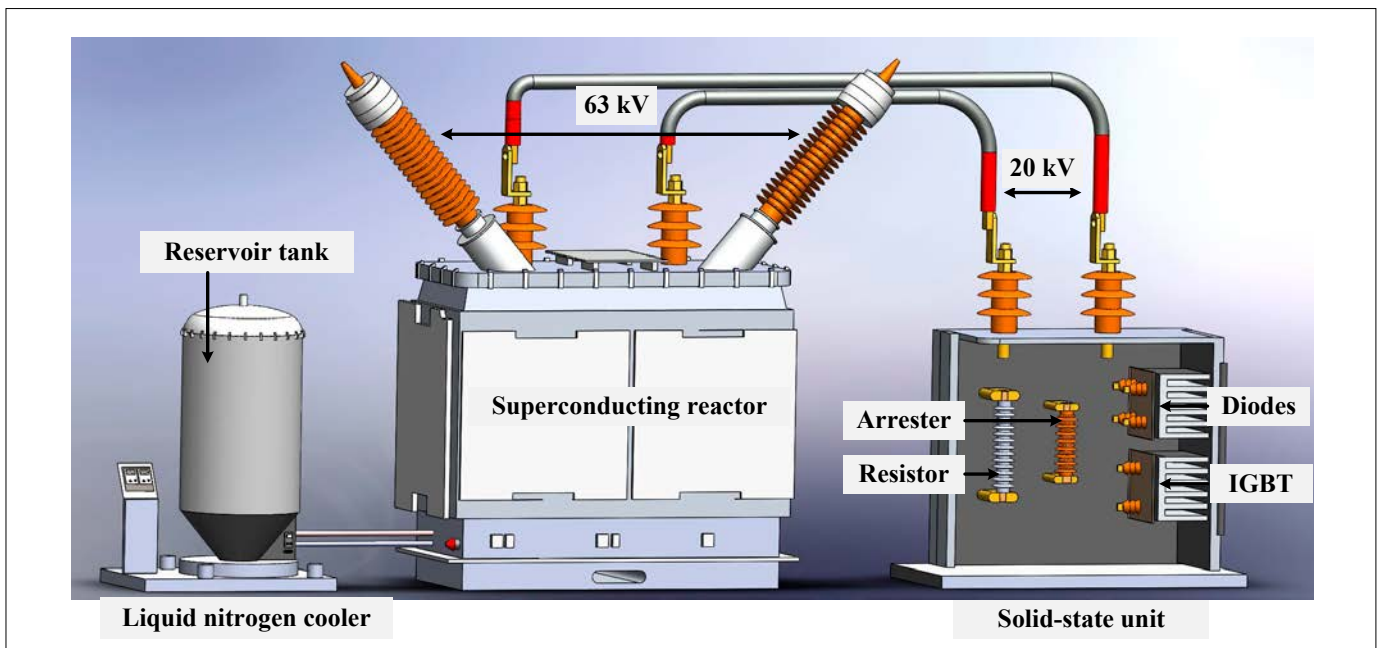


Figure 18. The primary scheme of CSSR implementation

[2] R. Rifaat, T. S. Lally, J. Hong, *Circuit breaker transient recovery voltage requirements for medium-voltage systems with NRG*, IEEE Transactions on Industry Applications, Vol. 50, No. 5, 2014

[3] *IEEE Guide for breaker failure protection of power circuit breakers*, IEEE Std C37.119-2016, 2016

[4] A. Heidary, H. Radmanesh, K. Rouzbehi, et al., *Inductive fault current limiters: A review*, Electric Power Systems Research, Vol. 187, 2020

[5] M. Noe, A. Hobl, P. Tixador, et al., *Conceptual design of a 24 kV, 1 kA resistive superconducting fault current limiter*, IEEE transactions on applied superconductivity, 22(3), 5600304-5600304, 2011

[6] W. Song, X. Pei, J. Xi, et al., *A novel helical superconducting fault current limiter for electric propulsion aircraft*, IEEE Transactions on Transportation Electrification, 2020

[7] B. Xiang, L. Gao, Z. Liu, Z., et al., *Short-circuit fault current-limiting characteristics of a resistive-type superconducting fault current limiter in DC grids*, Superconductor Science and Technology, 33(2), 024005, 2020

[8] M. Majka, J. Kozak, S. Kozak, et al., *Design and numerical analysis of the 15 kV class coreless inductive type SFCL*, IEEE Transactions on Applied Superconductivity, Vol. 25, No. 3, 2015

[9] J. Kozak, M. Majka, S. Kozak, et al., *Comparison of inductive and resistive SFCL*, in IEEE Transactions on Applied Superconductivity, Vol. 23, No. 3, 2013

[10] H. Kado, M. Ichikawa, M. Shibuya, et al., *Inductive type fault current limiter using Bi-2223 thick film on MgO cylinder with Bi-2212 buffer layer*, IEEE Transactions on Applied Superconductivity, Vol. 15, No. 2, 2005

[11] M. R. Barzegar, M. Niasati, *Fusion TRV limiter a solution to modify interrupting characteristics of CBs with presence of resonance type SFCL*, 2015 30th International Power System Conference (PSC), Tehran, Iran, 2015

[12] D. Huang, S. Shu, J. Ruan, *Transient recovery voltage distribution ratio and voltage sharing measure of double- and triple-break vacuum circuit breakers*, IEEE Transactions on Components, Packaging and Manufacturing Technology, Vol. 6, No. 4, 2016

[13] X. Cheng, Z. Chen, G. Ge, et al., *Dynamic dielectric recovery synergy of hy-*

brid circuit breaker with CO₂ gas and vacuum interrupters in series, IEEE Transactions on Plasma Science, Vol. 45, No. 10, 2017

[14] K. Funaki, Y. Sasasige, H. Yanagida, et al., *Development of low-AC-loss Bi-2223 superconducting multifilamentary wires*, IEEE transactions on applied superconductivity, 19(3), 3053-3056, 2009

Authors



Amir Heidary was born in Tabriz, Iran, in 1987. He received the BS and MS degrees from the Electrical Engineering Department of IAU, Iran, in 2012 and 2020, respectively. He has worked in Eleprotect Company as a researcher of electrical applications. From 2012 to 2021, his research was published in books, journal articles, and several patents. His invention won the award of the Iranian elite committee in 2014. Currently, he is the technical manager of the national project for the implementation of a series DC reactor in the Iran power grid. His fields of interest are power system protection, magnetic-based power applications, smart grids, and superconducting reactors.



Hassan Moradi CheshmehBeigi was born in Kermanshah, Iran, in 1979. He received his MS degree from the Faculty of Engineering, University of Shahid Beheshti, Tehran, Iran, in 2007. He received his Ph.D. degree in Electrical Engineering from the Shahid Beheshti, Tehran, Iran, in 2011. In 2011, he joined the University of Razi as an Assistant Professor in the Department of Electrical Engineering. His current research interests include novel electric motors and generators, electric machine drives and power electronic converters / inverters, renewable energy systems.



Ali Mehrizi-Sani received a Ph.D. degree from the University of Toronto in 2011. He is currently Associate Professor at Virginia Tech, Blacksburg, VA. His areas of interest include power system applications of power electronics and integration of renewable energy resources. He is an editor of IEEE Transactions on Energy Conversion, IEEE Power Engineering Letters, Energies, and MDPI Electronics. He was also an editor of IEEE Transactions on Power Systems, IEEE Transactions on Power Delivery, and Wiley International Transactions on Electrical Energy Systems (ITEES). He was the Chair of IEEE Task Force on Dynamic System Equivalents and Secretary of CIGRE Working Group C4.34 on Application of PMUs for Monitoring Power System Dynamic Performance. He is the recipient of the 2018 IEEE PES Outstanding Young Engineer Award, 2018 ASEE PNW Outstanding Teaching Award, 2017 IEEE Mac E. Van Valkenburg Early Career Teaching Award, 2017 WSU EECS Early Career Excellence in Research, 2016 WSU VCEA Reid Miller Excellence in Teaching Award, 2011 NSERC Postdoctoral Fellowship, and 2007 Dennis Woodford prize. He was a Connaught Scholar at the University of Toronto from 2007 to 2011.